# 2

# *Literature Review*

## 2.1 Transition Metal Dichalcogenides monolayer

$MX_2$ (M = transition metal and X = chalcogen atoms) is chemical formula of TMDs based 2D materials. These layers consist of a three-layered structure, where the top and bottom layers consist of chalcogen atoms and a middle layer made of transition metal. The TMDs mainly occur in two different crystal structures, hexagonal and trigonal. Some of the TMDs are naturally layered materials represented in Figure 2.1. In the hexagonal crystal structure, transition metal and chalcogen atoms are arranged into the trigonal prismatic symmetry. Moreover, in the trigonal crystal structure, transition metal and chalcogen atoms are arranged into octahedral symmetry. Figure 2.1 shows the schematic representation of the hexagonal and trigonal phase of $MoS_2$ monolayer and corresponding symmetry.

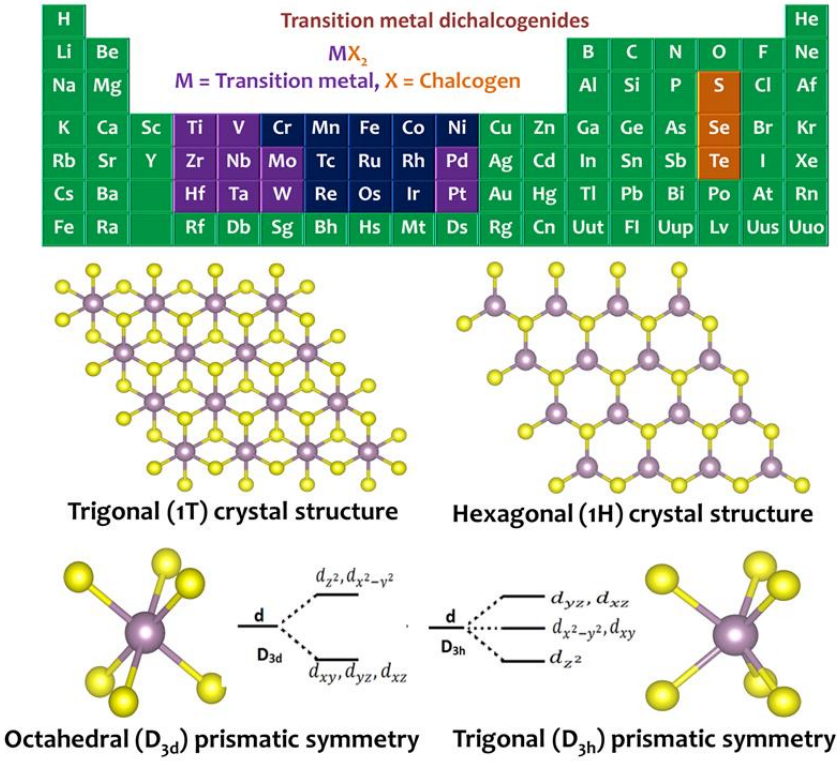


**Figure 2.1** Periodic table representing the possible transition metals and chalcogen atoms, top view of hexagonal and trigonal phase and corresponding possible symmetry

The outer cell electronic configuration of chalcogen atoms is $\boldsymbol{ns^2p_x^1p_y^1p_z^2}$, where s orbital is completely filled and two p-orbital having unpaired electrons and third p-orbital occupied by electrons. The filled $\boldsymbol{p_z^2}$ orbital called lone pair, and it may or may not participate in the bonding formation. Due to the completely filled s-orbitals, it is chemically inactive and didn't participate in the chemical bonding. In TMDs, the transition metal has six-fold symmetry, and chalcogen

atoms show three-fold symmetry, Figure 2.1. The transition metal complexes form the bonding between the empty orbitals and lone pairs of ligands. In TMDs, transition metal and chalcogen element have +4 and -2 charge, respectively. The lone pair of chalcogen atom sited at the $sp^3$-hybridized orbitals and terminated at the surface. The coordination of the chalcogenides is lopsided that's led to marked cleavage properties perpendicular to the hexagonal or trigonal symmetry axis. The absence of the dangling bonds on the surface makes these materials non-reactive and very stable.

### 2.1.1Synthesis methods of 2D TMDs

In general, there are two different approaches used for the synthesis of two-dimensional materials, described in the following sections.

#### Top-down approach

In this method, the size of the bulk materials is reduced to a few layers. There are various methods in this category. The mechanical exfoliation method is one of the most efficient methods for the synthesis of monolayer or multilayer from the bulk through the scotch tape. In the mechanical exfoliation method, a multilayer is peeled off from the bulk material through the adhesive scotch tape and brought this tape into contact with the substrate and rubbed to cleave them further. This method is useful for synthesizing the clean and high purity monolayer or multilayer for characterization and fabrication of nanodevices (Hai Li, Wu, Yin, & Zhang, 2014). The mechanical exfoliation method is useful only for layered structures. This method can't be used for scalable production. Moreover, it doesn't allow to control the size and thickness. Liquid exfoliation is another method for the synthesis of 2D materials.

In this method, the bulk powder is sonicated into a different solvent, and the obtained disperse solution is centrifuged. The dispersion of the monolayer or multilayer depends on the surface energy of the solvent that should be more than cohesive energy between the layers (Coleman et al., 2011). Ion intercalation is another approach for the synthesis method. In this method, the bulk material is submerged into the lithium-containing compound for a long time to intercalate. The water molecules react with the lithium atom and forming the $H_2$ gas, which leads to the separation of layers (Z. Zeng et al., 2012). This synthesis process may be used to produce significantly large up to submicron size monolayers. The electrochemical exfoliation method is also used for the synthesis of 2D materials. In this method, a DC bias is applied between the bulk material, and Pt electrode dipped into the solution (N. Liu et al., 2014). Initially, a lower bias is applied to wet the material followed by the high voltage for exfoliation of the bulk crystal.

#### Bottom-up approach

In this category, the 2D materials are synthesized by arranging atoms in a regular pattern, showing the minimum energy. Various methods are possible under this category. Chemical Vapor Deposition (CVD) is a widely used synthesis method for 2D materials. In this process, the substrate is heated, and transition metal and chalcogen precursors are evaporated simultaneously and transferred through the carrier gas, which finally deposits on the substrate. This method is used to synthesize a uniform film, and large scale production with excellent reproducibility is possible using it (Bosi, 2015). For these reasons, CVD is preferred for the synthesis of 2D materials. The second method is metal chalcogenisation. It is a two-step process. In the first step, few nanometers thin transition metal film deposited using the sputtering or e-beam evaporator and other physical vapor deposition methods on the substrate. In the second step, the chalcogenisation is performed on deposited transition metal thin film through CVD. This method is used for the controlled synthesis of 2D layered materials with a possibility for large scale synthesis. The other method is the chemical bath position that is the low-cost synthesis method for large scale production. The precursor of transition metal and chalcogen are dissolved into the water and add some acid/base for maintaining the pH of the solution. The substrate is dipped into the solution consisting of transition metal and chalcogen ions for some time and followed by

the chalcogenisation of materials using the CVD. Chemical bath deposition is one of the cost-effective and scalable methods for the synthesis of 2D materials (K. K. Liu et al., 2012).

### 2.1.2 Electronic properties

The electronic properties computed using the DFT and experimental techniques. Most of the bulks TMDs show indirect bandgap semiconductor nature, and when reduced down to monolayer, these showed direct bandgap semiconductor nature. Many researchers reported indirect to direct bandgap transition when the bulk material is reduced to monolayer; perhaps the first report was in 2010 (Mak, Lee, Hone, Shan, & Heinz, 2010). Theoretical calculation first predicted the direct bandgap nature at the K point of Brillouin zone (BZ) in $MoS_2$ and $WS_2$ monolayer. The bandgap of 2D materials is decreasing with increasing number of layers (Z. Y. Zhao & Liu, 2018). All monolayers based on group VI-B compounds exhibit direct band semiconductor with the gap lying the two inequivalent K and K'-points in BZ. The switching of direct band gap from bulk to monolayer is attributed to the interlayer hopping (Cappelluti, Roldán, Silva-Guillén, Ordejón, & Guinea, 2013). Band extrema points K, Γ, and Q in the valence band are splitting with increasing the number of layers that denotes the strength of hopping. The splitting at the Γ and Q point is relatively higher than the K point due to the fact the energy states at K point is contributed by transition metal d orbitals (Cui et al., 2013), Figure 2.2.

Moreover, energy states at Γ and Q point are dominated by p-orbital of chalcogen atom. However, the K point of valence band has negligible splitting due to interlayer splitting. The most important orbital contribution at the edge of the valence band at K-point is due to the combination of $d_{xy}$ and $d_{x2-y2}$ orbitals of the transition metal, which hybridize to $p_x$ and $p_y$ orbitals of the chalcogen atoms. Group VI-B compounds are the heavy element, so the spin-orbit coupling (SOC) is also an important parameter to consider. In the absence of SOC, states in the valence band at K-point doesn't show splitting. Moreover, if the SOC is considered, the pattern in the valence band at the K-point changes significantly. The bands at the K point in the valence band split into two degenerate manifolds because of the SOC and lack of inversion symmetry, shown in Figure 2.2. The magnitude mainly depends on the number of layers and transition metal present in TMDs. The splitting in Mo based TMDs is in the order of 150 meV and for heavy transition metal, W it increases up to 450 meV. Further, the electronic properties can be tailored using various ways including strain, electric field and heterostructure etc. in these materials.

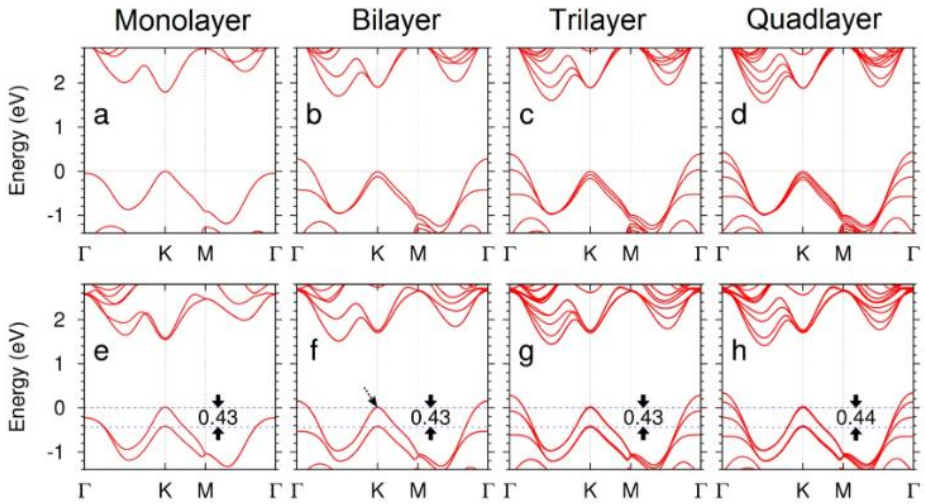


**Figure 2.2** Band gap variation of monolayer, bilayer, trilayer and quadlayer of $WS_2$ without and with SOC (Cui et al., 2013).

### 2.1.3 Optical properties

Group VI based TMDs monolayers exhibit direct bandgap characteristics, which include low to high bandgap systems, suitable for various optoelectronic applications. The carriers can

be excited from the valence band (VB) to conduction band (CB) by absorbing incident photons. Further, the excess carriers in the CB can also recombine, followed by light emission. The first process is known as light absorption, and the later is named as photoluminescence. These are schematically shown in Figure 2.3(a). The phonons also contribute to the optical properties, in which the emitted photon may have lower/higher energy compared to the incident photons. The variation in the energy of the emitted photon is correlated with specific phonon modes. This inelastic process is known as Raman scattering, shown in Figure 2.3(b).

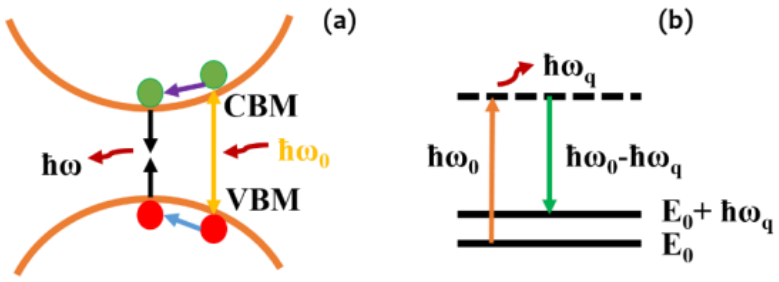


**Figure 2.3**Schematic representations of (a) light absorption and photoluminescence and (b) Raman scattering. (Incident light energy – $\hbar\omega_0$, emitted light energy – $\hbar\omega$ and emitted phonon energy – $\hbar\omega_q$)

All the TMDs monolayers exhibit two low energy peaks in the absorption spectra due to the excitonic features associated with the interband transition at the K(K′) point of BZ (Kastner, 1972). These peaks are arising due to valence band (VB) splitting by considering the SOC. At higher energy around room temperature, these two merged into one peak (Ross et al., 2013).

### 2.1.4 Modification in electronic and optical properties

The TMDs based monolayers can be strained by more than 10% strain without breaking the crystal structure (Bertolazzi, Brivio, & Kis, 2011).

It is the simplest way to tune the electronic properties for various applications. Three fold-symmetry makes them attractive to tailor the properties at small strain compared to six fold-symmetry in graphene (Z. H. Ni et al., 2008). Tensile strain reduces the bandgap of TMDs monolayer and turns into an indirect bandgap (Johari & Shenoy, 2012), shown in Figure 2.4. Further increasing the strain above 10% strain, bandgap closes (Gan & Zhao, 2014). The TMDs based monolayer can sustain more strain (Bertolazzi et al., 2011) than the Si (Petersen, 1982), thus, these materials are very useful for flexible optoelectronic devices.

The electric field is another approach and the safest way to modify the properties of the materials without breaking the symmetry and crystal structure. It can change the electronic properties of materials. Moreover, the optical properties like the absorption coefficient and refractive index can be modified. The transverse electric field significantly reduces the band gap of the bilayer of TMDs. The bandgap of the TMDs bilayers continuously decreases with increasing the electric field and even closes at a specific electric field (Xiao et al., 2014). The electric field required for semiconductor to metal transition decreases from S to Te due to the diffuse nature of valence $p_z$ orbitals from S to Te, which facilitates more charge transfer from chalcogen atom to transition metal at the same level of the electric field. Due to the presence of the electric field, the spin degeneracy is observed in the valence band of $MoS_2$ bilayer system. The electric field localizes the charges along the direction of the applied field, thus, confining charges to the atomic plane, but delocalized charges within these planes causes the semiconductor to metal transitions.

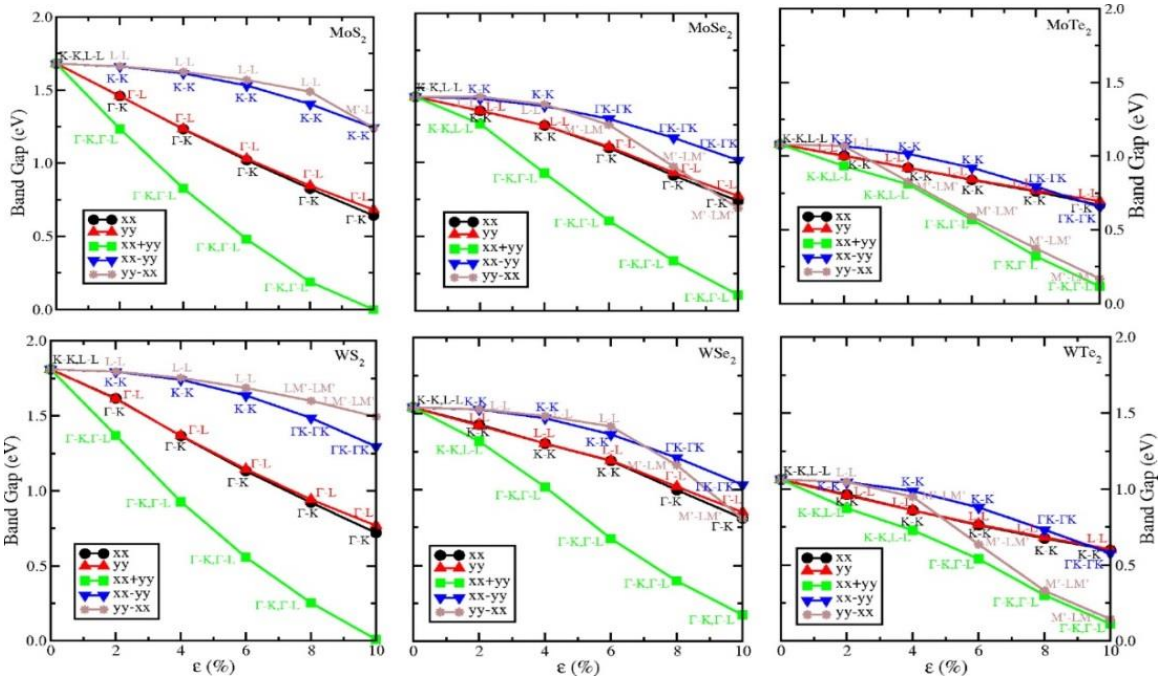


**Figure 2.4** Bandgap variation against the uniaxial and biaxial strain of $MX_2$ (M = Mo, W; X = S, Se, and Te) monolayers (Johari & Shenoy, 2012)

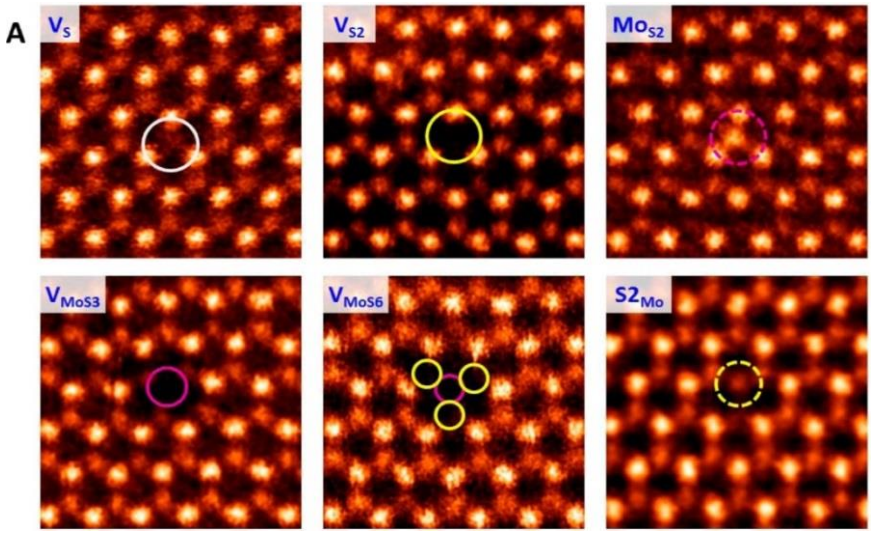


**Figure 2.5** Point defects and antisite defects observed in $MoS_2$monolayer using the STM analysis (W. Zhou et al., 2013a)

The TMDs based 2D materials are defect prone systems. The defects are created during the growth process, the monolayer transfer process, and electron irradiation. Various types of defect, dislocation, and grain boundaries are observed experimentally (W. Zhou et al., 2013a) and shown in Figure 2.5. These defects introduce the defect states in the forbidden region and also shift the Fermi energy, affecting the electronic properties of materials. The defects in the TMDs can be saturated by doping of transition metal that will provide a new opportunity to tune the materials properties. These defects play important roles to control/degrade the performance of the electronic device. For example, in case of gas sensing applications, these defects provide an active site to adsorb the gas molecule and thus, improve the gas sensing response. Various point defects are studied in $MoS_2$ monolayer grown by (CVD) using the atomic resolution annular dark field imaging on an aberration corrected Scanning Tunneling Microscope (STM) and DFT calculation. The most commonly observed point defects sulfur vacancy (Vs), disulfur vacancy ($V_{S2}$), complex

vacancy ($V_{MoS3}$ and $V_{MoS6}$), and antisite ($S_{2Mo}$ and $Mo_{S2}$). More insight about the electronic properties, DFT studies are carried out. The stability of the point defect is evaluated in terms of the formation energy; Vs defect included monolayer has the lowest formation energy which confirms the maximum probability of this defect in monolayer. The similar observations are also observed experimentally. The electronic band structure of defect included monolayer is also modified and additional states are populating in the bands due to the presence of defects.

### 2.1.5 Applications

The TMDs based monolayers are known for their exceptional physical and chemical properties. These properties inspired researchers to explore such systems for various application including, solar cell, piezoelectric, gas sensor, biosensor, chemical sensor, field effect transistor, water splitting, and energy storage. Figure 2.6 shows the schematic representation of the potential applications of TMDs monolayers and respective device structures.

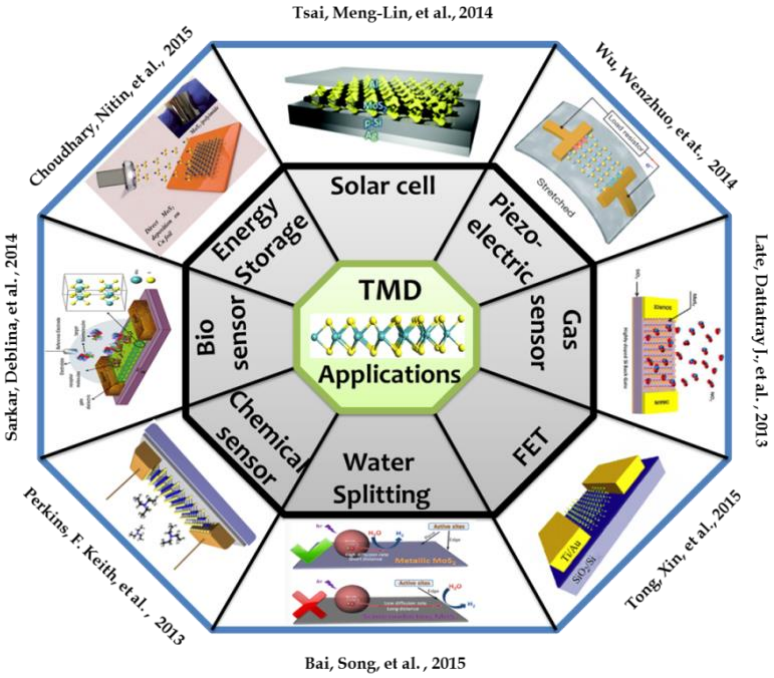


**Figure 2.6** Schematic representation of applications of TMDs based monolayers

## 2.2 Janus Transition Metal Dichalcogenides monolayer

Recently, a new class of TMDs based 2D material, Janus MoSSe monolayer has been synthesized using the chemical vapor phase transport method (Lu et al., 2017; Jing Zhang et al., 2017). Janus TMDs (JTMDs) monolayers have chemical formula MXY, where M is transition metal and X and Y are the two different chalcogen elements, having different atomic radii and inequivalent atomic bond length, leading to the change in the M-X and M-Y bond lengths. Janus monolayers break the reflection symmetry intrinsically and possess the trigonal $C_{3v}$ crystal symmetry. The broken mirror symmetry facilitates the out-of-plane band splitting and in plane Rashba effect. The parent TMDs have centrosymmetry due to two similar chalcogen element, while Janus monolayers are non-centrosymmetric due to two different chalcogen element. The asymmetric nature along two chalcogen elements breaks the mirror symmetry which induces the intrinsic dipole on transition metal in the out-of-plane direction leading to internal electric field. The size of the dipole and internal electric field depend on the various factors but strongly depend on the difference in electronegativity of chalcogen X and Y atoms. It has been observed that almost all the Janus monolayers for valleytronics have hexagonal unit cell therefore 2H and 1T phase of Janus with $C_{3v}$ symmetry is considered.

### 2.2.1 Synthesis method

There is minimal literature, and we came across only two reports on the fabrication of Janus MoSSe monolayer. Li and coworkers reported the synthesis of Janus MoSSe though the selenization of $MoS_2$ monolayer fabricated using CVD method (Lu et al., 2017). Figure 2.7(a) shows the synthesis steps of Janus MoSSe monolayer. In the first step, $MoS_2$ monolayer triangular flakes are synthesized using the CVD method. In the second step, the top layer of sulfur atoms is replaced by the hydrogen atom first using the hydrogen plasma without breaking the vacuum, and MoSH structure is formed. In the last step, the top layer of the hydrogen atom is replaced by selenium atoms through the thermal selenization without breaking the vacuum and finally fabricated Mo-S and Mo-Se covalently bonded Janus MoSSe monolayer. The hydrogen plasma power is very critical for replacing the top layer of sulfur atoms by hydrogen atoms without breaking the bottom Mo-S covalent bond. Also, thermal selenization temperature is critical to replace the top layer of hydrogen with selenium atoms without disturbing the bottom layer of sulfur atoms. The substrate temperature for thermal selenization should lie in the range of 350 to 450$^0$C.

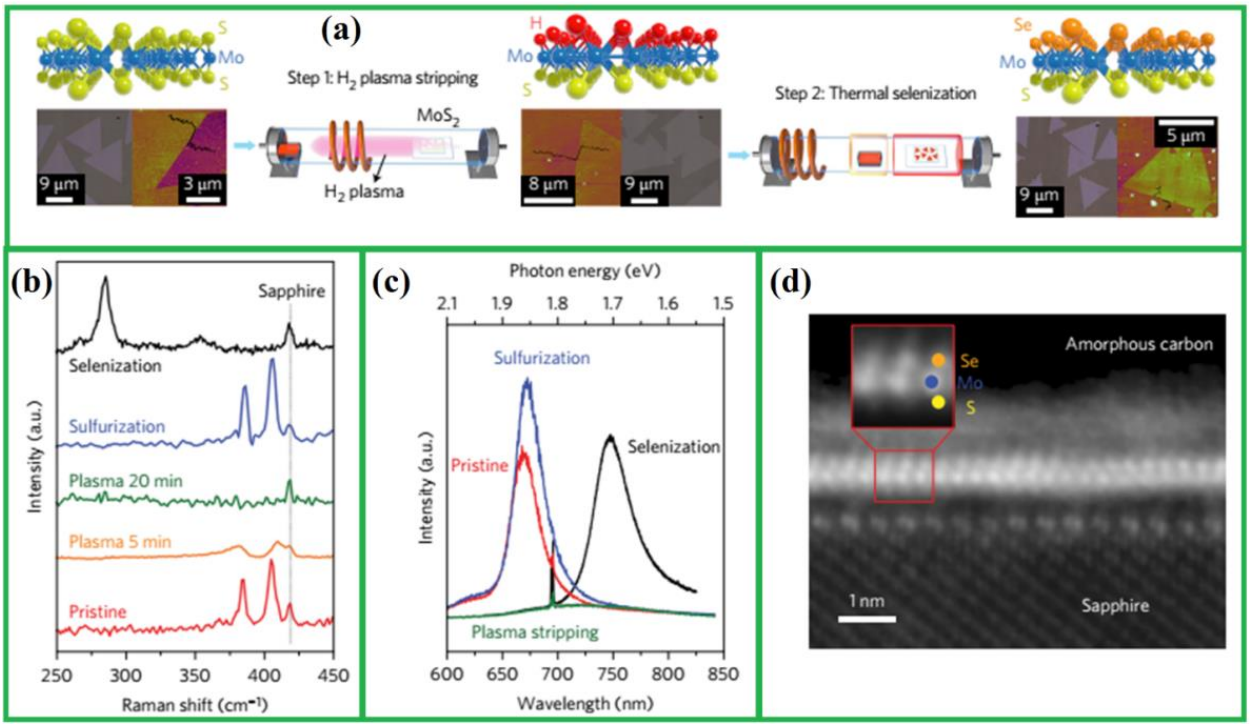


**Figure 2.7** (a) Steps used for synthesis process, (b) Raman spectrum, (c) Photoluminescence spectrum and (d) Angular dark field STEM of MoSSe monolayer (Lu et al., 2017)

Moreover, the random MoSSe structures are found after thermal selenization above 600$^0$C. The optical image and atom force microscopy image for each step is shown in Figure 2.7(a). The vertical height for $MoS_2$ monolayer found around 1.0 nm and 0.7 to 0.8 nm found for MoSH monolayer. The reduced vertical height represents the strip off the top of the sulfur layer and formation of top of the H layer. Stable Janus MoSSe monolayer showed ~ 1.1 nm vertical height. The experimentally obtained vertical height has been validated from the DFT results. The formation of $MoS_2$, MoSH, and Janus MoSSe monolayer is validated from respective Raman spectra, shown in Figure 2.7(b). The Raman frequencies of out-of-plane and in-plane modes are 406 cm$^{-1}$ and 387 cm$^{-1}$, respectively. The Raman vibrational modes vanished corresponding to the 20 min stripping of hydrogen plasma, confirming the formation of MoSH. After the thermal selenization of MoSH, out-of-plane vibrational modes shifted to 288 cm$^{-1}$, and in-plane vibrational modes shifted to 355 cm$^{-1}$. These shifted peaks substantiate the formation of MoSSe monolayer. This is in agreement with the calculated phonon band dispersion. The optical band gap of $MoS_2$

monolayer calculated is around 1.88 eV using the photoluminescence spectrum. The MoSH monolayer showed the metallic nature, in agreement with the DFT results. The photoluminescence of Janus MoSSe monolayer shows a peak at 1.68 eV, which is close to the average of $MoS_2$ and $MoSe_2$ monolayer bandgap value. Figure 2.7(d) illustrates the cross-sectional annular dark image from STEM validates the asymmetry in the top and bottom layer and thus, substantiating the formation of Janus MoSSe monolayer.

### 2.2.2 Janus monolayers properties and applications

The electronic properties of group VI based JTMDs are explored computationally and experimentally. It is observed that all such systems exhibit direct bandgap semiconductor except MoSTe and WSTe monolayers. The bandgap of monolayers lies in between the bandgap of parent monolayers. The reasonable bandgap and very high mobility attracted researchers to explore these monolayers for nanoelectronic devices. The broken mirror symmetry in Janus monolayers induces the Rashba splitting in the topmost VB. The magnitude of Rashba splitting depends on the transition metal and potential gradient. Due to the coexistence of the SOC and broken mirror symmetry, Janus MoSSe monolayer has multivalleyed band structure and strong correlation between the spin and valley physics (Peng, Ma, Zhang, Huang, & Dai, 2018). The doping of the transition metal, Cr/V introduced the strong valley polarization with 60 meV energy difference, and it is improved by applying strain engineering. The Janus monolayers have intrinsic built in electric field due to the broken mirror symmetry, which may assist in separating the photogenerated electron-hole pairs (X. Ma, Wu, Wang, & Wang, 2018). These monolayers properties ensure that the Janus monolayers have a potential for use in water-splitting photocatalyst applications. The out-of-plane piezoelectric polarization in Janus monolayers is also reported (Dong, Lou, & Shenoy, 2017). The strong in-plane and weak out-of-plane piezoelectric polarization observed is attributed to the uniaxial strain. The out-of-plane piezoelectric polarization is enhanced by creating a multilayer. These piezoelectric properties provide a platform for nanodevices. The theoretically explored applications of JTMDs are shown in Figure 2.8. However, many more applications are yet to explore in coming future, and that is what a question mark (?) section signify.

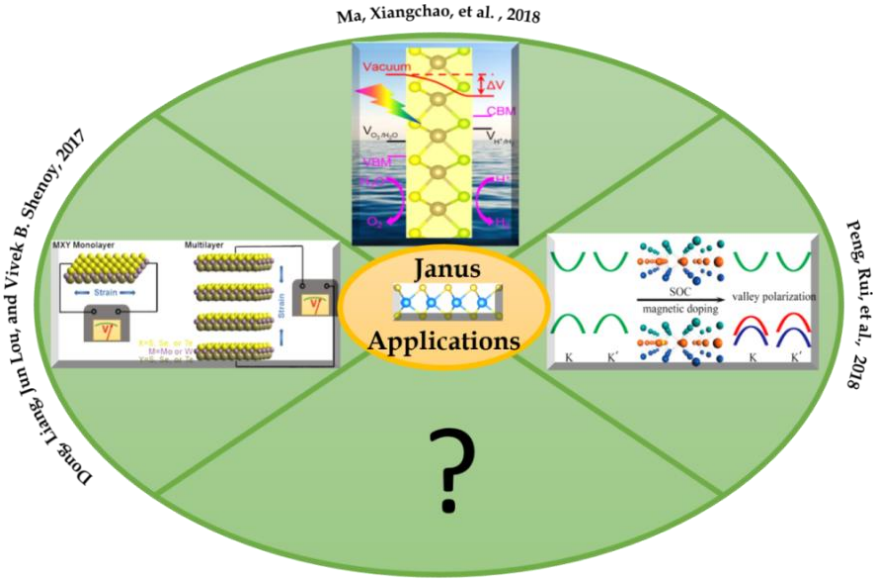


**Figure 2.8** Theoretically explored applications of JTMDs monolayers.